SUPPORTING INFORMATION

1. Elemental analysis

The chemical composition of $CuRh_2Sb$ and $NiRh_2Sb$ synthesized with the polyol process as well as the high-temperature method has been analyzed by EDX spectroscopy. The average values and standard deviation of each sample are shown in Table S1 and Table S2. The spectra and elemental distribution maps of $CuRh_2Sb$ and $NiRh_2Sb$ nanoparticles are shown in Figure S1.

Table S1. EDX data of $CuRh_2Sb$ synthesized with polyol process and high-temperature method at different points.

$CuRh_2Sb$(*tI*8) nanoparticle from polyol process				Polycrystalline $CuRh_2Sb$ from high-temperature synthesis			
Point	Cu	Rh	Sb	Point	Cu	Rh	Sb
1	24.94	48.43	26.63	1	26.24	49.75	24.02
2	22.69	51.56	25.74	2	26.48	49.47	24.05
3	25.62	47.71	26.67	3	26.84	49.59	23.57
4	25.32	49.47	25.20	4	26.45	48.98	24.57
5	27.16	48.4	24.44	5	26.05	49.24	24.71
6	23.28	51.53	25.19	6	26.27	49.46	24.27
7	23.25	51.05	25.7	7	24.78	49.77	25.45
8	22.75	50.87	26.37	8	26.46	49.20	24.34
9	24.40	50.27	25.33	9	26.84	49.05	24.11
10	26.17	48.66	25.18	10	26.77	48.66	24.57
11	23.3	52.00	24.7	11	25.22	49.69	25.09
12	23.99	48.01	28.00	12	26.37	48.97	24.66
13	25.61	47.29	27.1	13	26.96	48.81	24.23
Average	24.5	49.6	25.9	Average	26.3	49.3	24.4
σ	1.4	1.6	1.0	σ	0.6	0.4	0.5

Table S2. EDX data of $NiRh_2Sb$ synthesized with polyol process and high-temperature method at different points.

$NiRh_2Sb$ nanoparticle from polyol process				Polycrystalline $NiRh_2Sb$ from high-temperature synthesis			
Point	Ni	Rh	Sb	Point	Ni	Rh	Sb
1	24.53	50.33	25.14	1	25.37	49.30	25.33
2	23.60	50.92	25.47	2	25.03	47.53	27.44
3	23.06	51.26	25.68	3	26.35	48.52	25.13
4	24.97	49.80	25.23	4	26.16	48.74	25.10
5	24.74	49.86	25.40	5	25.75	49.32	24.93
6	23.67	50.82	25.50	6	26.10	49.08	24.82
7	24.90	49.67	25.44	7	26.06	48.39	25.56
8	24.60	50.33	25.07	8	26.30	48.75	24.95
9	24.33	50.24	25.43	9	26.37	48.85	24.78
10	23.38	50.74	25.89	10	26.18	48.71	25.11
11	23.68	50.84	25.48	11	25.76	48.96	25.27
12	23.75	50.51	25.73	12	25.28	49.62	25.11
Average	24.1	50.4	25.5	Average	25.9	48.8	25.3
σ	0.6	0.5	0.2	σ	0.4	0.5	0.7

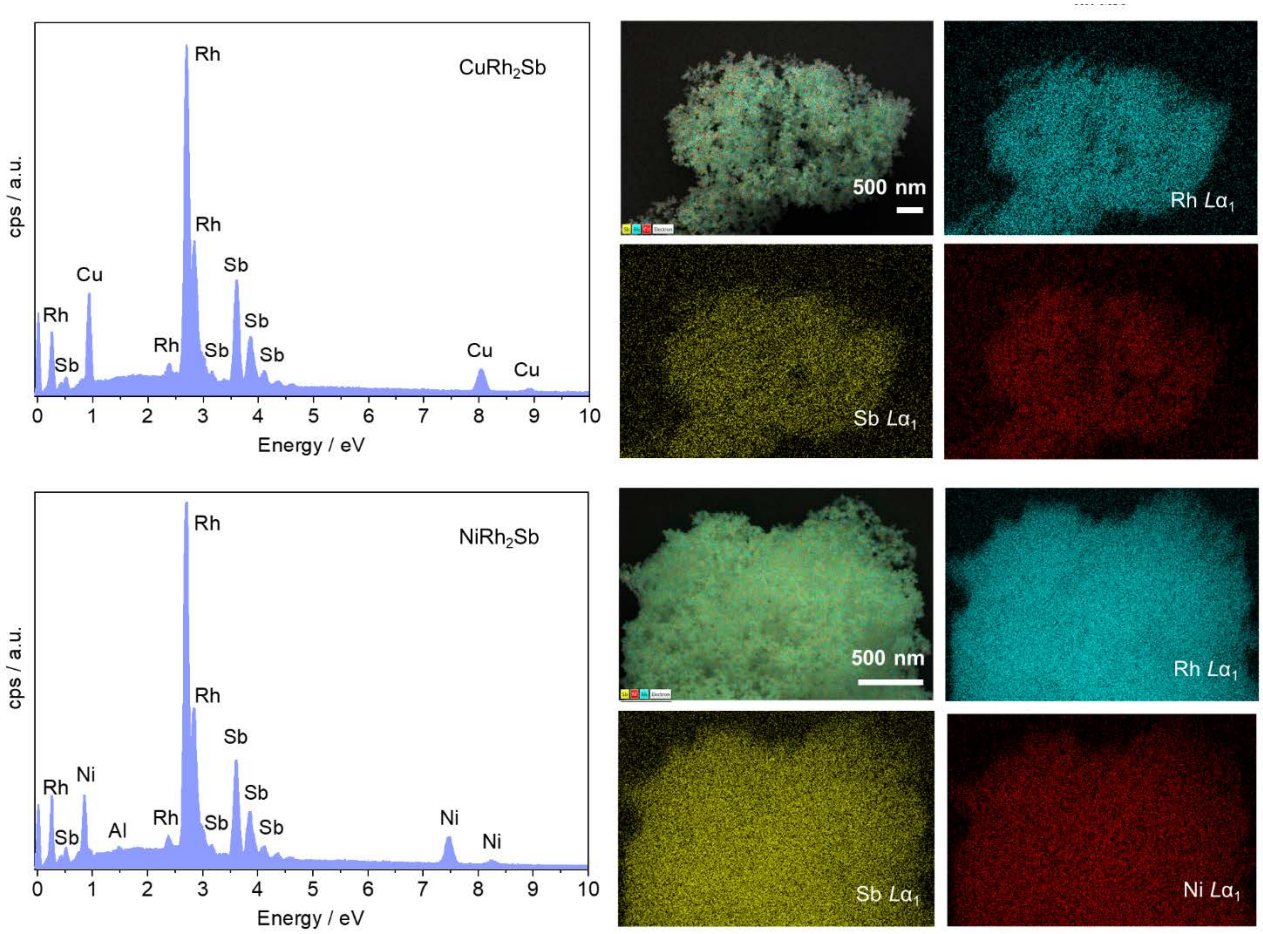

Figure S1. EDX spectra and elemental distribution maps of $CuRh_2Sb$ (top) and $NiRh_2Sb$ (bottom) nanoparticles. The signal of aluminum came from the aluminum stab.

2. Nanoparticle growth on carbon cloth

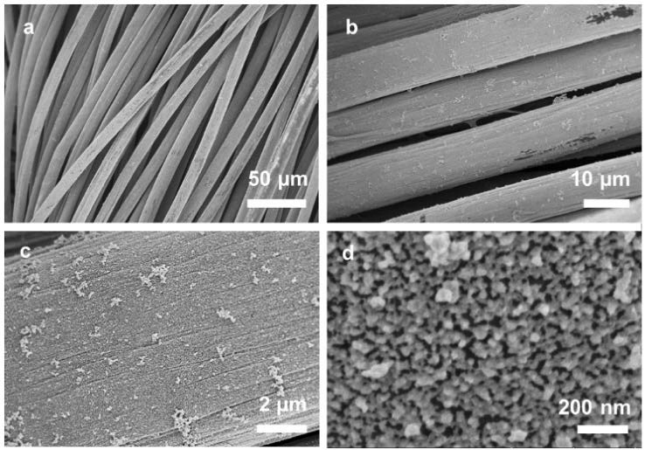

Figure S2. SEM images showing homogeneous growth of $CuRh_2Sb$(*tI*8) nanoparticles on carbon cloth at different magnification: (a) 500 times, (b) 2000 times, (c) 10 000 times, (d) 100 000 times.

3. Annealing of nanoparticles

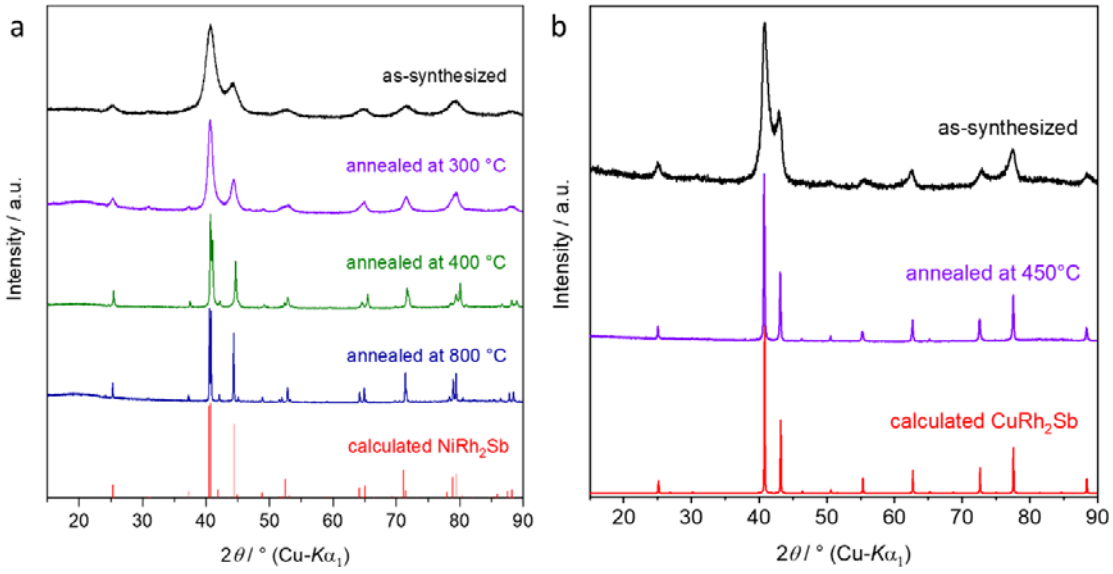

Figure S3. PXRD measurements of as-synthesized and annealed products of (a) $NiRh_2Sb$ and (b) $CuRh_2Sb$(*tI*8). The calculated pattern is simulated with the crystal structure solution in Table S3–S5.

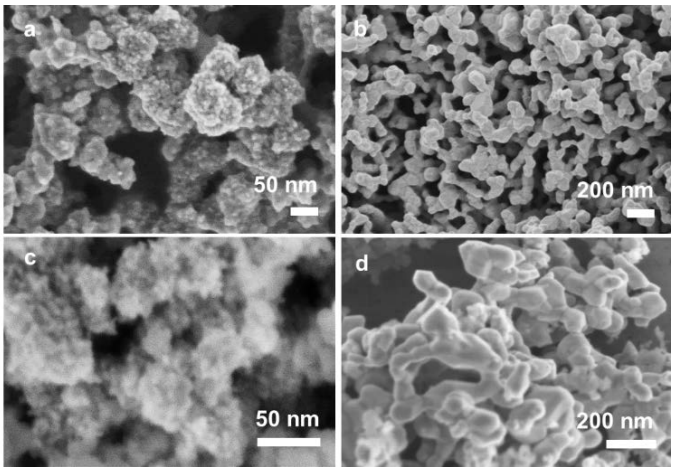

Figure S4. SEM images. (a) As-synthesized $NiRh_2Sb$ nanoparticles. (b) $NiRh_2Sb$ nanoparticles after annealing at 400 °C for 6 days. (c) As-synthesized $CuRh_2Sb$(*tI*8) nanoparticles. (d) $CuRh_2Sb$(*tI*8) nanoparticles after annealed at 400 °C for 5 days.

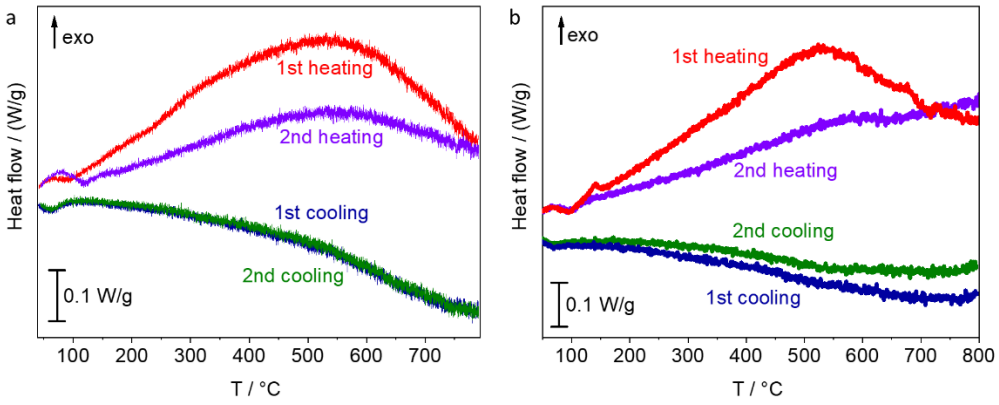

Figure S5. DSC measurements of the annealing process of (a) $NiRh_2Sb$ and (b) $CuRh_2Sb$ nanoparticle. Two circles of ramping from room temperature to 800 °C were carried out, during which no phase transition appeared. The first and the second heating round do not overlap, which may indicate the growth of the crystal size during the first heating process.

4. Crystal structure

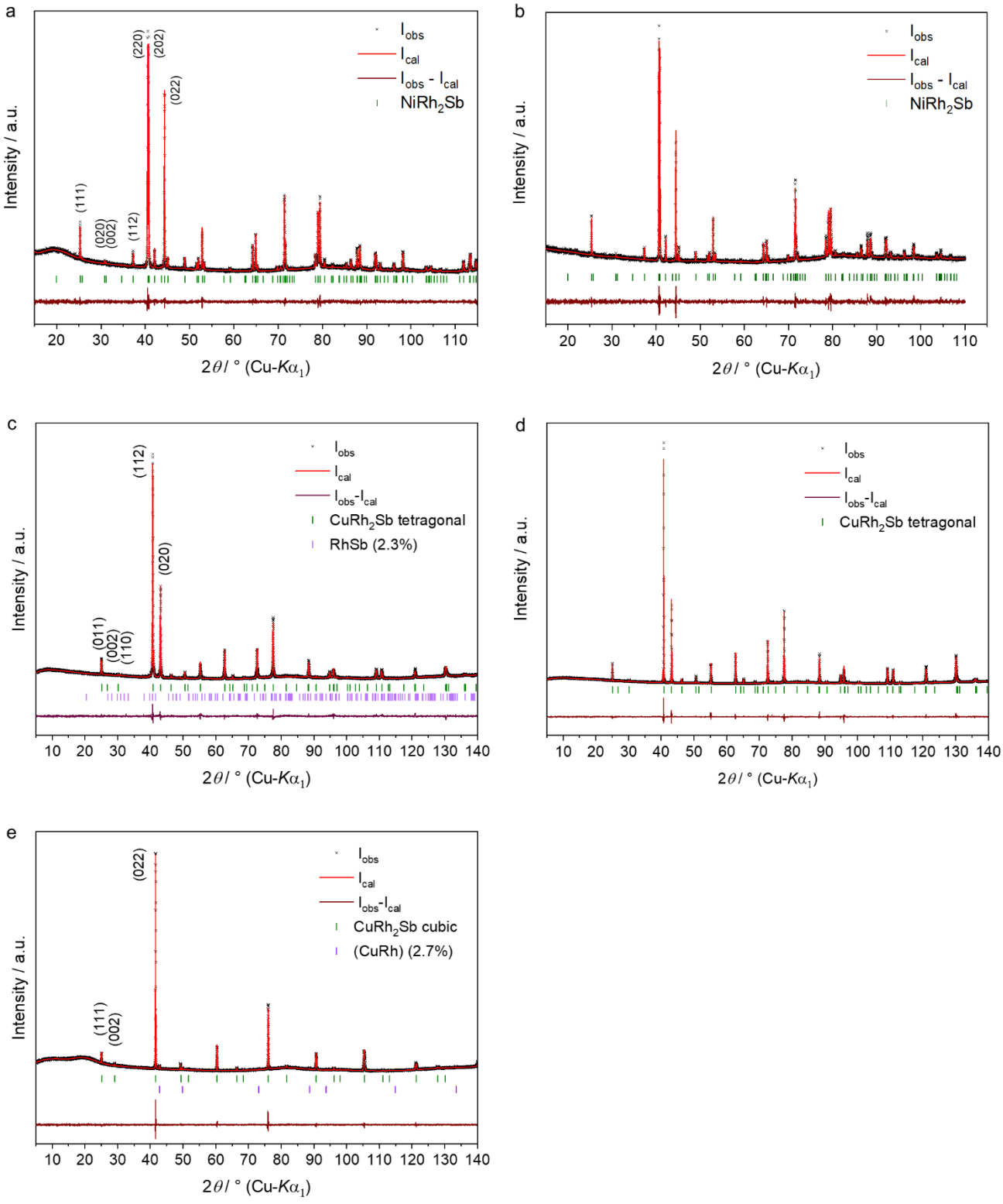

Figure S6. Rietveld refinement plot of (a) annealed $NiRh_2Sb$ nanoparticle, (b) high-temperature synthesized $NiRh_2Sb$, (c) annealed $CuRh_2Sb$(*tI*8) nanoparticle with 2.3% by-product (RhSb, ICSD-76621), (d) high-temperature synthesized tetragonal $CuRh_2Sb$(*tI*8), and (e) high-temperature synthesized cubic $CuRh_2Sb$(*cF*16) with 2.7% by-product (CuRh, ICSD-108403). The peak positions of the target structures are marked by green vertical bars, and by-products by violet vertical bars.

Table S3. Crystallographic and Rietveld refinement data of annealed $NiRh_2Sb$ nanoparticle, annealed $CuRh_2Sb$(*tI*8) nanoparticle, and polycrystalline $CuRh_2Sb$(*cF*16). *R* values are as defined by the *TOPAS Academic V5* manual.[46,47]

Empirical formula	$NiRh_2Sb$		$CuRh_2Sb$		
Crystal system	**orthorhombic**		**tetragonal**		**cubic**
Space group (no.)	*Cmcm* (no. 63)		*I*4/*mmm* (no. 139)		*Fm*$\bar{3}$*m* (no. 225)
Pearson symbol	*oC*16		*tI*8		*cF*16
Synthesis	polyol process	high-temperature	polyol process	high-temperature	high-temperature
a / Å	6.9188(1)	6.9150(1)	4.1859(1)	4.1828(1)	6.1235(1)
b / Å	5.7917(1)	5.7902(1)	4.1859(1)	4.1828(1)	6.1235(1)
c / Å	5.7374(1)	5.7311(1)	6.6375(1)	6.6492(2)	6.1235(1)
V / Å^3	229.91(1)	229.48(1)	116.30(1)	116.33(1)	229.62(1)
Z	4	4	2	2	4
Formula weight	386.26	386.26	391.12	391.12	391.12
ρ_{calc} / g cm^{-3}	11.16(1)	11.18(1)	11.17(1)	11.17(1)	11.31(1)
T / K	296(1)	296(1)	296(1)	296(1)	296(1)
Radiation λ / Å	1.5406	1.5406	1.5406	1.5406	1.5406
2θ range / °	15 to 115	5 to 110	5 to 140	5 to 120	5 to 140
Step width / °	0.013	0.007	0.013	0.013	0.013
Data points	7691	15000	10385	8847	10385
R_p	0.04187	0.05746	0.04046	0.03998	0.03074
R_{wp}	0.05423	0.07452	0.05359	0.05999	0.04189
R_{exp}	0.05573	0.07409	0.04764	0.03901	0.03927
Goodness of fit	0.973	1.006	1.125	1.538	1.066

Table S4. Wyckoff positions, coordinates, and displacement parameters (/Å) for the atoms in $NiRh_2Sb$ and $CuRh_2Sb$.

	Atom	site	*x*	*y*	*z*	SOF	B_{eq}
$NiRh_2Sb$	Sb	4*c*	0	0.2733(4)	0.25	1	0.62
	Rh	8*e*	0.2260(1)	0	0	1	0.72
	Ni	4*c*	0	0.7228(8)	0.25	1	0.70
	Atom	Site	*x*	*y*	*z*	SOF	B_{eq}
$CuRh_2Sb$ (*tI*8)	Sb	2*a*	0	0	0	1	2.10
	Rh	4*d*	0	0.5	0.25	1	2.07
	Cu	2*b*	0	0	0.5	1	2.56
	Atom	site	*x*	*y*	*z*	SOF	B_{eq}
$CuRh_2Sb$ (*cF*16)	Cu	4*a*	0	0	0	1	1.13
	Rh	8*c*	0.25	0.25	0.25	1	0.64
	Sb	4*b*	0.5	0.5	0.5	1	0.91

Table S5. Interatomic distances in $NiRh_2Sb$.

Atom #1	Atom #2	Symmetry code	*d* / Å
Rh	Sb	x, y, z	2.647
Rh	Sb	1/2+x, -1/2+y, z	2.716
Rh	Ni	x, -1+y, z	2.661
Rh	Ni	1/2+x, -1/2+y, z	2.705
Rh	Rh	x, y, 1/2-z	2.869
Rh	Rh	1/2-x, 1/2-y, -z	2.915
Rh	Rh	-x, -y, -z	3.127
Sb	Ni	x, y, z	2.603
Sb	Ni	-x, 1-y, 1/2+z	2.869
Sb	Ni	x, -1+y, z	3.189

Table S6. Interatomic distances in $CuRh_2Sb$(*tI*8).

Atom #1	Atom #2	Symmetry code	*d* / Å
Rh	Cu	x, y, z	2.671
Rh	Rh	-y, x, z	2.960
Rh	Sb	x, y, z	2.671
Cu	Sb	1/2+x, 1/2+y, 1/2+z	2.960
Cu	Sb	x, y, z	3.319

Table S7. Interatomic distances in $CuRh_2Sb$(*cF*16).

Atom #1	Atom #2	Symmetry code	*d* / Å
Rh	Cu	x, y, z	2.652
Rh	Rh	-y, x, z	3.062
Rh	Sb	x, y, z	2.652

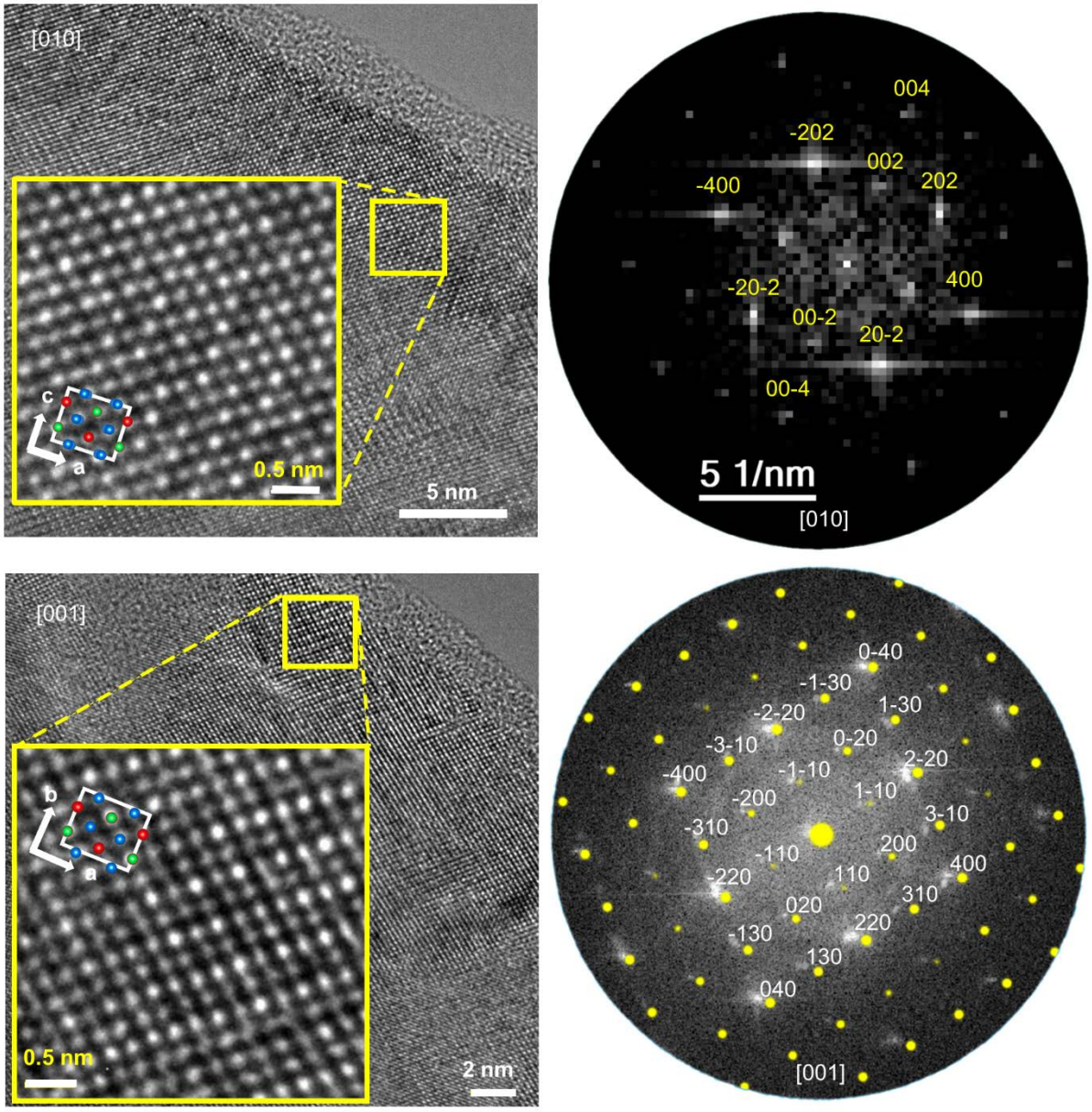

Figure S7. HRTEM images and diffractograms (i.e., Fourier transforms) of high-temperature synthesized $NiRh_2Sb$ crystals in [010] (top) and [001] (bottom) orientations. The simulated electron diffraction pattern overlayed in yellow in the bottom diffractogram is deliberately slightly displaced in order not to obscure the experimental data. Legend for atomic model: red sphere = Sb, blue sphere = Rh, green sphere = Ni.

5. $CuRh_2Sb$ phase transition

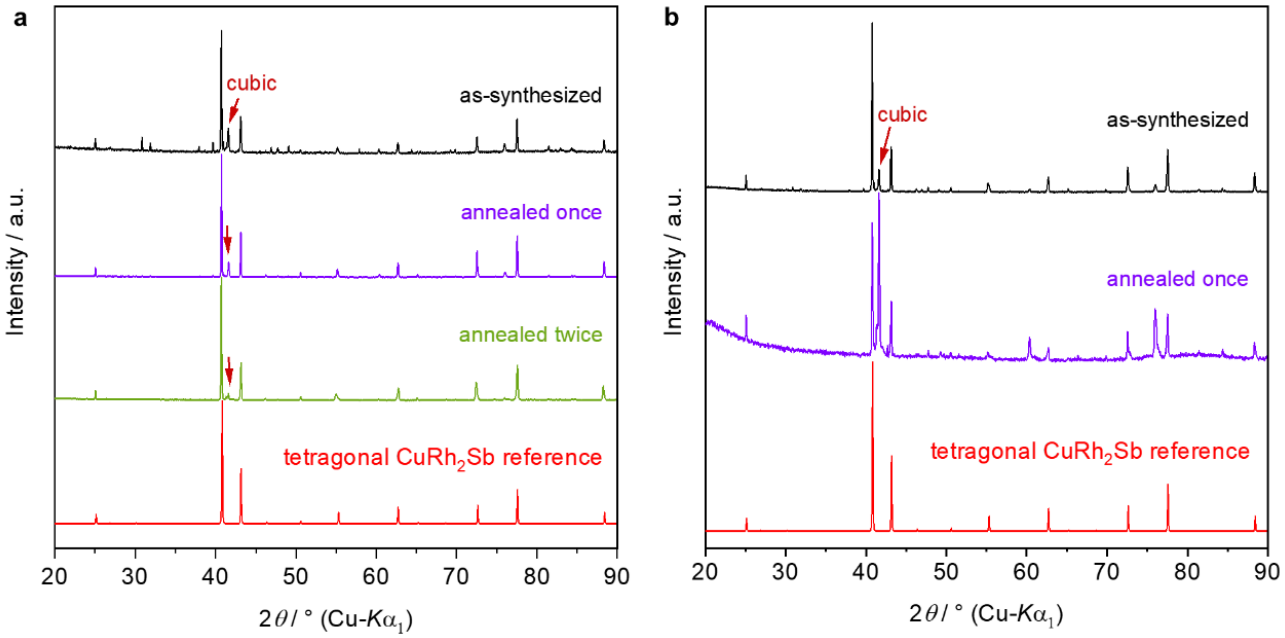

Figure S8. $CuRh_2Sb$ phase transition. (a) The as-synthesized sample is a mixture of $CuRh_2Sb$(*tI*8) as a major and $CuRh_2Sb$(*cF*16) as a minor constituent (plus traces of RhSb). In the first annealing step, the sample was heated to 800 °C at a rate of 60 K h^{-1}, cooled down at a rate of –5 K h^{-1} to 438 °C, and then quenched to ambient temperature. This product was then annealed for a second time, heated to 850 °C at a rate of 120 K h^{-1}, kept at that temperature for 2 days, and quenched. After both processes, the ratio of the tetragonal to the cubic phase amount has increased. (b) The as-synthesized sample is a mixture of $CuRh_2Sb$(*tI*8) as the major and $CuRh_2Sb$(*cF*16) as the minor phase. It was heated to 800 °C at a rate of 60 K h^{-1} and kept at that temperature for 4 days, then cooled down at a rate of –16 K h^{-1} to room temperature. After annealing, the ratio of the tetragonal to the cubic phase has decreased.

6. Air-stability

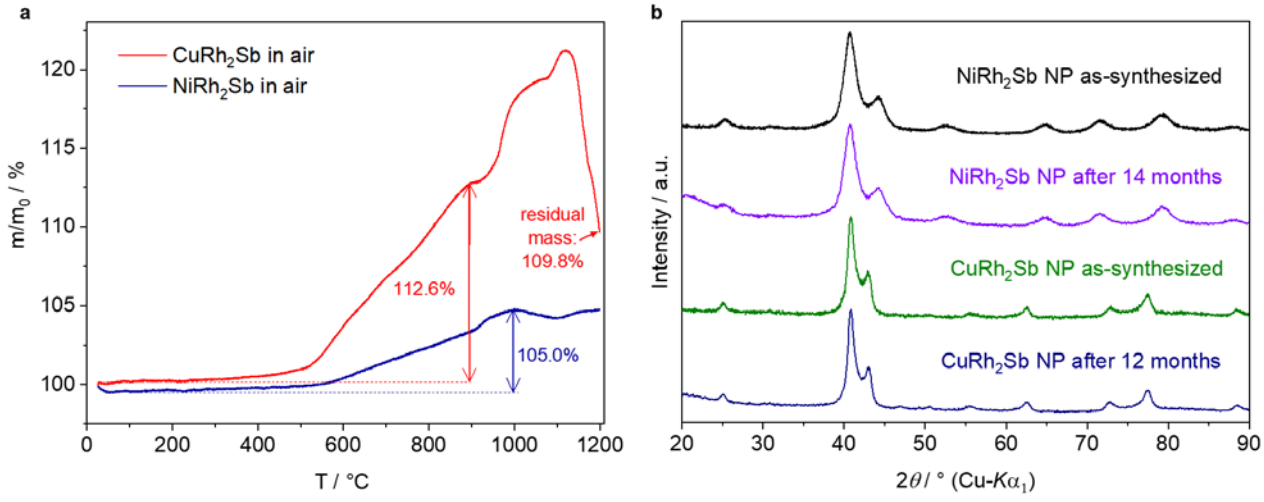

Figure S9. (a) TGA measurements for polycrystalline $NiRh_2Sb$ and $CuRh_2Sb$(*tI*8) in open Al_2O_3 crucibles until 1200 °C. (b) PXRD measurements showing the structure of $NiRh_2Sb$ and $CuRh_2Sb$(*tI*8) nanoparticles to be stable after being stored in air under ambient conditions for one year.

7. Calculated electronic structure

The influence of the spin-orbit interaction on the band structure of tetragonal $CuRh_2Sb$(*tI*8) is presented in Figure S10 and Table S8. Without spin-orbit interaction, several band crossings (marked in red) appear close to the Fermi energy (Figure S10a, c), while they are removed when the spin-orbit interaction is respected (Figure S10b, d).

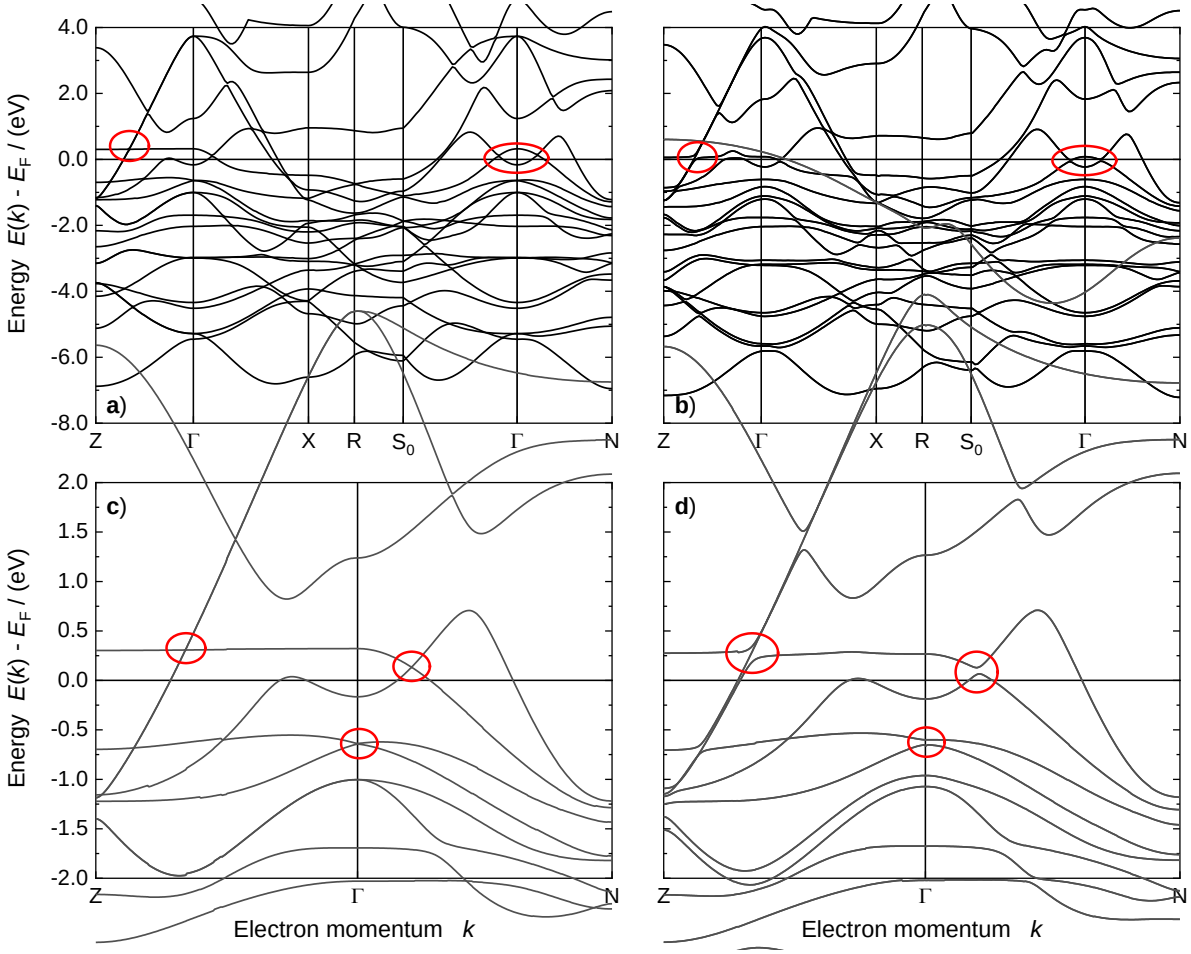

Figure S10. Band structure of tetragonal $CuRh_2Sb$(*tI*8). (a) and (c) are calculated without spin-orbit interaction, while in (b) and (d), spin-orbit interaction is included. (c) and (d) are shown for a smaller part in *k*-space with a higher point density.

The irreducible representations for the valence and conduction states (bands) closest to the Fermi energy at the Γ point are tabulated in Table S8. The point group at Γ is D_{4h}.

Table S8. Band characters.
Tabulated are band number (No.), degeneracy (*d*), Energy (E-E_F), and irreducible representation (irrep) of the valence and conduction bands in the vicinity of E_F at the Γ point determined with and without spin-orbit coupling (SOC).

Without SOC			
No.	*d*	E - E_F [eV]	irrep
55	1	-0.87785	Γ3+ *B1g*
57	1	-0.59426	Γ4- *B2u*
59	1	-0.22562	Γ1+ *A1g*
E_F		0	
61	1	0.0939	Γ1- *A1u*

With SOC			
No.	*d*	E - E_F [eV]	irrep
28	2	-0.82764	Γ7+ *E3/2g*
29	2	-0.60841	Γ7- *E3/2u*
30	2	-0.22834	Γ6+ *E1/2g*
E_F		0	
31		0.08083	Γ6- *E1/2u*

The Bader charges have been determined from a QTAIM (quantum theory of atoms in molecules) analysis and are summarized in Table S9. The results are accurate within 0.01 and do not change within this limit if spin-orbit interaction is respected or not. About 0.5 electrons are transferred to the Rh atom.

Table S9. Bader charges of cubic and tetragonal $CuRh_2Sb$.
Tabulated are the ions and their nuclear charge (Z), the number of valence electrons N_e in the Bader basins, and the resulting charge $Q = Z - N_e$. The values are extracted from calculations including spin-orbit interaction.

		Cubic		Tetragonal	
Atom	Z	N_e	Q	N_e	Q
Rh	45	45.457	–0.457	45.463	–0.463
Cu	29	28.675	0.325	28.663	0.337
Sb	51	50.405	0.595	50.411	0.589

In the case of orthorhombic $NiRh_2Sb$, the Bader charges were determined to be –0.418 (Rh), 0.264 (Ni), and 0.573 (Sb). The charge transfer is in the same order of magnitude as obtained for $CuRh_2Sb$. The band structure and the accompanied density of states ($n(E)$) calculated without spin-orbit interaction are shown in Figure S11.

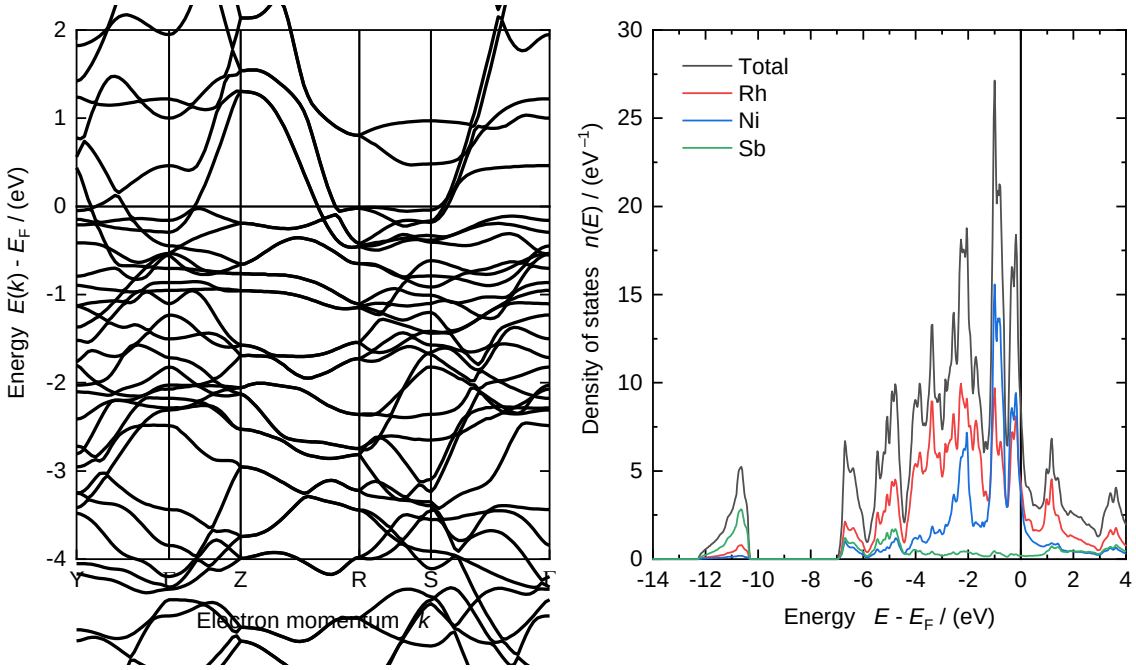

Figure S11. Calculated electronic structure of orthorhombic $NiRh_2Sb$.

8. XPS measurements

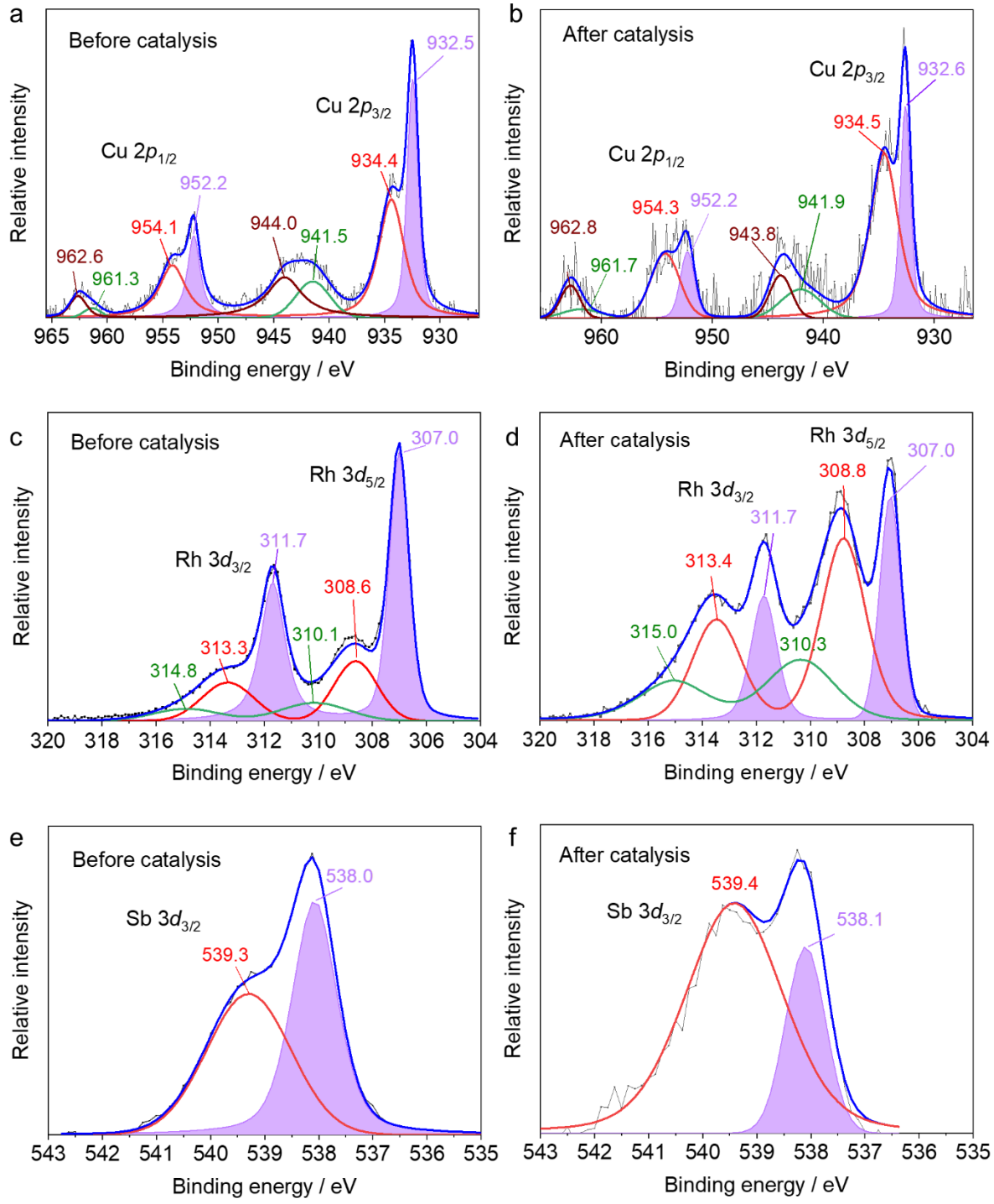

Figure S12. XPS measurements of Cu 2*p*, Rh 3*d* and Sb 3$d_{3/2}$ states in $CuRh_2Sb$(*tI*8) nanoparticles. (a, c, e) show the measurements with as-synthesized nanoparticles, and (b, d, f) are measured with the nanoparticle collected from the carbon cloth electrode after electrochemical catalysis for 50 hours. The violet areas present the elements in metal states, while the red lines show an oxidized state of the elements. The green and the brown peaks in Cu 2*p* are satellites from the oxide (red) [1], and the green peaks in Rh 3*d* are for an oxidized state.

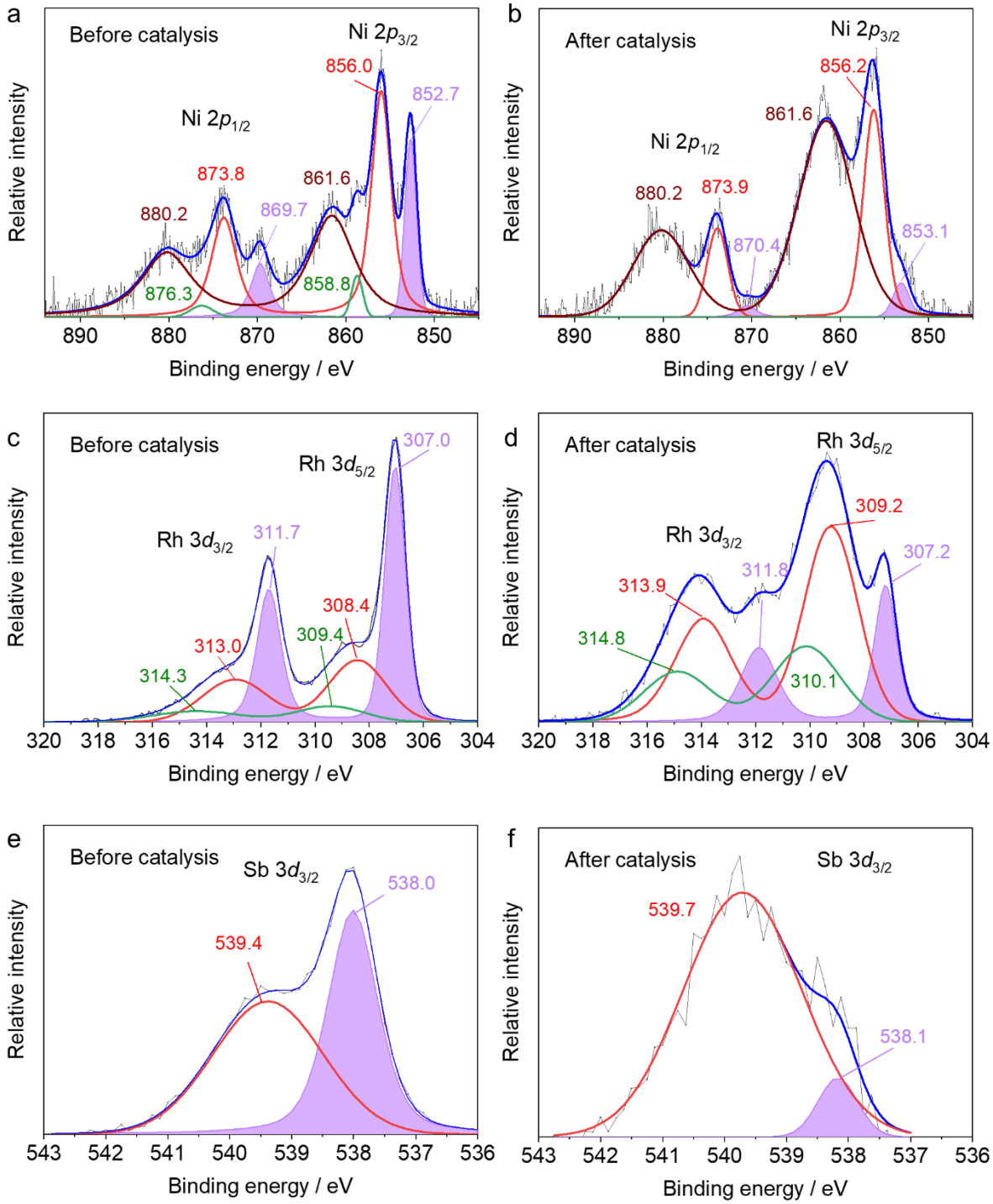

Figure S13. XPS measurements of Ni 2*p*, Rh 3*d,* and Sb $3d_{3/2}$ of $NiRh_2Sb$ nanoparticles. (a, c, e) show the measurements with as-synthesized nanoparticles and (b, d, f) are measured with the nanoparticle collected from the carbon cloth electrode after electrochemical water splitting for 25 hours. The violet areas present the elements in metal states, while the red lines show an oxidized state of the elements. The green and the brown peaks in Ni 2*p* are satellites from the oxide (red), and the green peaks in Rh 3*d* are for an oxidized state.

Table S10. Percentage of the metal state in all species of each element, considering the green lines in Figures S12 and S13 to be an oxidized state.

$CuRh_2Sb$(*tI*8)			$NiRh_2Sb$		
Spectra	Before CA	After CA	Spectra	Before CA	After CA
Cu 2*p*	33%	25%	Ni 2*p*	16%	4%
Rh 3*d*	61%	29%	Rh 3*d*	53%	21%
Sb $3d_{3/2}$	50%	24%	Sb $3d_{3/2}$	46%	8%

9. Electrochemical characterization

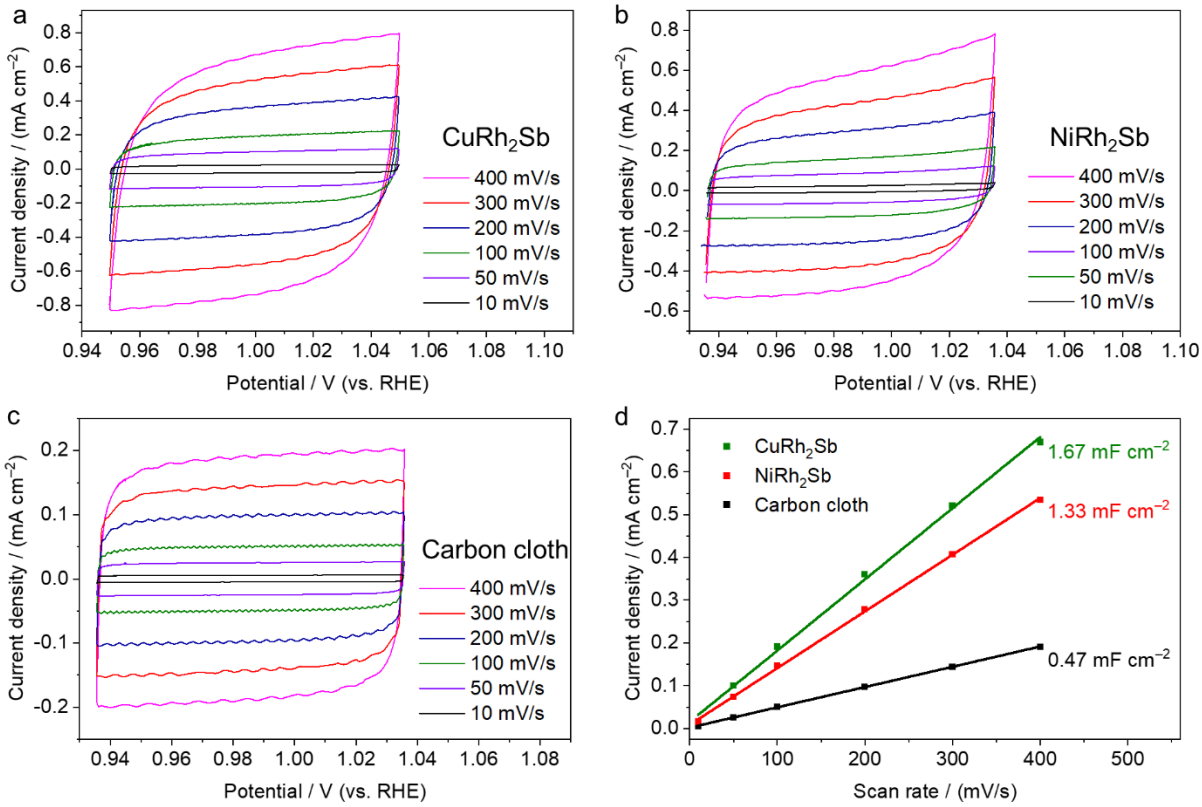

Figure S14. (a–c) CV curves with scanning rates of 10–400 mV/s in the open circuit on electrodes loaded with $CuRh_2Sb$(*tI*8), $NiRh_2Sb$ or without catalyst. (d) Evaluation of C_{dl} showing both catalysts increasing ECSA drastically.

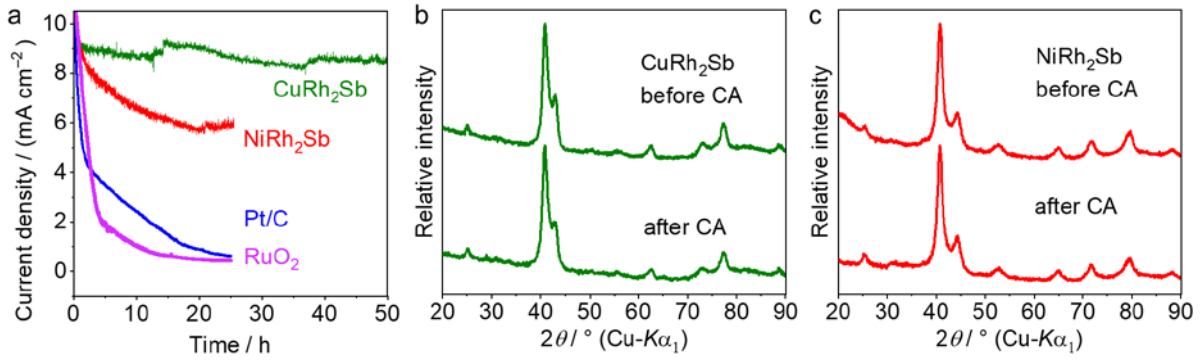

Figure S15. (a) CA curves for $NiRh_2Sb$ and $CuRh_2Sb$(*tI*8). (b, c) PXRD patterns before and after CA experiments for $CuRh_2Sb$(*tI*8) and $NiRh_2Sb$, showing no change in the crystal structures of the catalysts.

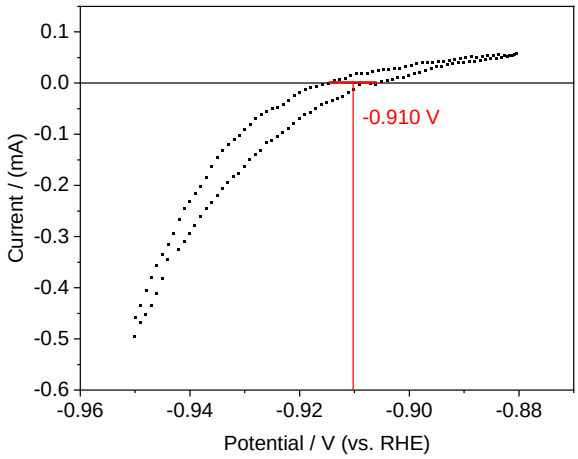

Figure S16. Calibration curve of the Hg/HgO reference electrode with respect to RHE carried out in 1 M KOH solution with Pt plates as the working electrode and the counter electrode at a scan rate of 1 mV s^{-1}. The solution is hydrogen saturated and the working electrode is constantly purged with hydrogen during the measurement. In the CV curve, the middle of the two potentials at which the current crossed zero was taken to be the thermodynamic potential.[2, 3]

References

[1] M. C. Biesinger, *Surf. Interface Anal.* **2017**, 49, 1325.
[2] S. Niu, S. Li, Y. Du, X. Han, P. Xu, *ACS Energy Lett.* **2020**, *5*, 1083.
[3] Y. Liang, Y. Li, H. Wang, J. Zhou, J. Wang, T. Regier, H. Dai, *Nat. Mater.* **2011**, 10, 780.